2. System description

Figure 2 shows the block diagram of the proposed lidar system. The optical signal and the LO are split from the same CW laser source. The LO branch is directly connected to the receiver and the transmitted signal is modulated through an electro-optic I/Q modulator. The modulating RF signals from a digital arbitrary waveform generator (AWG) are fed to the I and the Q channels of the modulator independently. Optical carrier suppression and sideband rejection ratio are optimized by properly adjusting the DC bias of the modulator. As a result, a constant frequency modulation at f_{CW} is loaded onto the lower optical sideband and a wideband saw-tooth chirping signal is loaded onto the upper optical sideband. The modulated optical signal is amplified by an erbium doped fiber amplifier (EDFA), and a polarization controller (PC) behind the EDFA adjusts the state of polarization of the optical signal to match the principle axis of the 2x2 fiber-optic polarization beam splitter (PBS) connected to the telescope. A quarter wave plate is placed in front of the telescope to create a 90° polarization rotation for each roundtrip. Thus the optical signal reflected from the target and enters the telescope will pass through the PBS with minimum attenuation before it reaches the receiver through the adjacent fiber port. In the receiver, the optical signal is combined with the LO through a 2x2 fiber-optic 90° hybrid which allows the separation of the inphase and the quadrature components in the optical signal with two photodetectors. After photodetection, electrical signals are sampled by a pair of high speed analog-to-digital converters (ADC) before they are analyzed through digital signal processing.

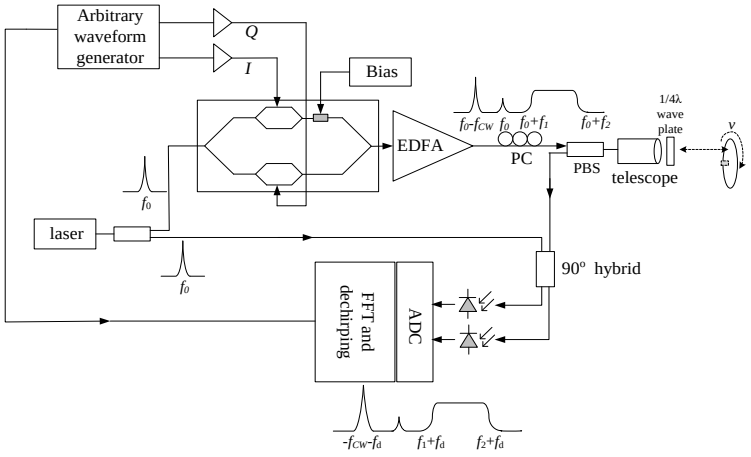

Fig. 2. Block diagram of the proposed lidar system.

To create a wideband chirp waveform which linearly sweeps from f_1 to f_2 on the upper optical sideband, and a constant frequency modulation at f_{CW} on the lower optical sideband, the two voltage waveforms used to drive I and Q arms of the I/Q modulator are [10],

$$V_I(t) = V_D\left[\cos(2\pi f_1 t + \pi\frac{f_2 - f_1}{T}t^2) - \sin(2\pi f_{CW}t)\right] \tag{4}$$

$$V_Q(t) = V_D\left[-\sin(2\pi f_1 t + \pi\frac{f_2 - f_1}{T}t^2) + \cos(2\pi f_{CW}t)\right] \tag{5}$$

where, V_D is the amplitude of the driving voltage signal. When both intensity modulators (I and Q branches) inside the I/Q modulator are biased at null point, and the phase shifter is biased at the quadrature point, the optical field at the output of the modulator is [11]

#175888 - $15.00 USD Received 10 Sep 2012; revised 20 Oct 2012; accepted 22 Oct 2012; published 1 Nov 2012

$$E_0 = E_s\left[\sin\left(\frac{\pi V_I(t)}{V_\pi}\right)\cos(2\pi f_0 t) + \sin\left(\frac{\pi V_Q(t)}{V_\pi}\right)\sin(2\pi f_0 t)\right] \quad (6)$$

where f_0 is the optical frequency of the CW laser, E_s is the constant input optical field and V_π is the voltage required for the transfer function to change from the minimum to the maximum for each intensity modulator. For small-signal modulation, $V_D / V_\pi \ll \pi$, Eq. (6) can be linearized to

$$E_0 \approx E_s\left[\cos\left[2\pi\left(f_0 + f_1 + \frac{f_2 - f_1}{2T}t\right)t\right] + \sin(2\pi f_0 t - 2\pi f_{CW} t)\right] \quad (7)$$

This is a carrier suppressed optical signal with independent modulating signals carried on the upper and the lower sidebands. Since the optical LO is not modulated, its optical field can be expressed as,

$$E_{LO} = A_{LO}\cos(2\pi f_0 t) \quad (8)$$

where, A_{LO} is the field amplitude. The optical field reflected from the target E_{sig} contains a time delay Δt and a Doppler frequency shift f_d compared to the launched optical field given by Eq. (7), so that,

$$E_{sig} = A_{sig}\left[\cos\left[2\pi\left(f_0 + f_1 + \frac{f_2 - f_1}{2T}(t-\Delta t) + f_d\right)t\right] + \sin(2\pi f_0 t - 2\pi f_{CW} t - 2\pi f_d t)\right] \quad (9)$$

Where, A_{sig} is the amplitude of the reflected optical field. Sending E_{LO} and E_{sig} into the two input ports of the 90 degree optical hybrid, the optical fields E_1 and E_2 exiting the two output ports can be described by

$$\begin{pmatrix} E_1 \\ E_2 \end{pmatrix} = \frac{1}{\sqrt{2}}\begin{pmatrix} 1 & \exp\left(j\frac{\pi}{4}\right) \\ \exp\left(j\frac{\pi}{4}\right) & 1 \end{pmatrix}\begin{pmatrix} E_{sig} \\ E_{LO} \end{pmatrix} \quad (10)$$

Photocurrents of the two photodetectors after the 90° optical hybrid are,

$$I_{arm1} = \Re|E_1|^2 = \Re A_{LO}A_{sig}\left\{\cos\left[2\pi\left(f_1 + \frac{f_2 - f_1}{2T}(t-\Delta t) + f_d\right)t - \frac{\pi}{4}\right] - \sin\left(2\pi f_{CW}t + 2\pi f_d t + \frac{\pi}{4}\right)\right\} \quad (11)$$

$$I_{arm2} = \Re|E_2|^2 = \Re A_{LO}A_{sig}\left\{-\sin\left[2\pi\left(f_1 + \frac{f_2 - f_1}{2T}(t-\Delta t) + f_d\right)t - \frac{\pi}{4}\right] + \cos\left(2\pi f_{CW}t + 2\pi f_d t + \frac{\pi}{4}\right)\right\} \quad (12)$$

where $\Re$ is the responsivity of the photodetector, and terms due to direct detection have been neglected for simplicity. Because these two photocurrent signals represent the real and the imaginary parts of the optical signal, the complex optical signal can be recovered in the electrical domain as,

$$\begin{aligned} I_{final} &= I_{arm1} - jI_{arm2} \\ &= \Re A_{LO}A_{sig}\left\{\exp\left[j2\pi\left(f_1 + \frac{f_2 - f_1}{2T}(t-\Delta t) + f_d\right)t - j\frac{\pi}{4}\right]\right. \\ &\quad \left. -\exp\left[j(-2\pi f_{CW}t - 2\pi f_d t + \frac{\pi}{4})\right]\right\} \end{aligned} \quad (13)$$

#175888 - $15.00 USD Received 10 Sep 2012; revised 20 Oct 2012; accepted 22 Oct 2012; published 1 Nov 2012

The complex optical spectrum can be obtained through a fast Fourier transform (FFT) on this composite electrical signal I_{final}, in which the positive and the negative sidebands represented by the 1st and the 2nd terms on the RHS of Eq. (13) are not redundant. Doppler frequency shift f_d can be obtained directly from the negative sideband, while the positive sideband corresponds to the time-delayed saw-tooth chirping signal. De-chirping can be applied by mixing the positive sideband with the original chirping waveform to find the de-chirped frequency f_R and the target range. In this process, the Doppler frequency shift f_d can be easily subtracted to make the range measurement accurate.

3. Experiment

The transmitter used in the lidar system experiment was built based on a Ciena commercial optical transmitter which was originally designed for 10Gb/s optical transmission with electronic domain pre-compensation [11]. Two 21.42GS/s digital-to-analog converters (DAC) with 6-bit resolution were equipped in the transmitter, which converted the digital modulation signal to analog format to drive the two RF ports of the I/Q modulator. The amplitude of the RF modulating signal can be varied by adjusting the gain of the two RF power amplifiers after the DACs. This transmitter has a 15-bit long internal digital memory so that the maximum temporal length of the arbitrary waveform generated by this transmitter was 1.5298μs. The bandwidth of the I/Q modulator used in the experiment was 10GHz. An integrated tunable laser assembly (Emcore TTX1994) was used as the CW laser source with 100kHz spectral linewidth, The laser wavelength was set at 1549.65nm in the experiment.

The optical signal from the transmitter was collimated onto a spinning disc through free-space optics. The surface of the disc is covered with retro-reflective tape so that the reflected optical signal can be easily collected. The disc was placed approximately 1.6m away from the telescope. The velocity seen by the laser beam can be adjusted by changing either the beam position along the radius of the disc, or the angle between the laser beam and the disc surface normal. Note that the velocity is zero if the disc surface normal is in the same direction of the laser beam, the sign of the velocity seen by the laser can also be flipped through this angle change. The spinning speed of the disc is approximately 2316 rpm (revolutions per minute) and the beam position on the disc is about 4.5cm off the center.

In the receiver, two wideband photodiodes were used after the 90 degree optical hybrid both with 30GHz bandwidth. A real-time oscilloscope (LeCory 8600A) with 20Gs/s sampling rate and approximately 6GHz analog bandwidth was utilized as the ADCs after the RF pre-amplifiers which digitally record the two detected signals. Then the digital signals were processed using a MATLAB program to extract the velocity and range information.

To simultaneously measuring the speed and the distance, two different modulation signals were loaded independently onto the upper and the lower optical sidebands. The upper sideband was loaded with a saw-tooth linear chirping as shown in Fig. 1(a) with 4.3GHz chirping bandwidth. A raised cosine window function was applied to the chirping signal to minimize the edge effect on each optical pulse. The pulse repetition period was $T' = 1.5298\mu s$, and pulse duration was $T = 0.6884\mu s$. The lower sideband was loaded with a single frequency modulation at $f_{CW} = 5.3545GHz$, which corresponds to a maximum measurable non-aliasing velocity of 4.149km/s. For the signal on the lower sideband, the pulse width equals to the repetition period *T'* so that the amplitude of the sinusoid is constant. The selection of modulation frequency at $f_{CW} = 5.3545GHz$ minimizes the phase discontinuity between data frames. The dashed curve in Fig. 3 shows the signal optical spectrum measured by an optical spectrum analyzer (OSA) with 0.01 nm spectral resolution. The solid trace in Fig. 3 was the same optical spectrum but measured with a coherent heterodyne technique by mixing the optical signal with another narrow linewidth laser whose central frequency was approximately 6 GHz away from that of the signal laser. The heterodyne spectrum shown in Fig. 3 was acquired through an RF spectrum analyzer so that

#175888 - $15.00 USD Received 10 Sep 2012; revised 20 Oct 2012; accepted 22 Oct 2012; published 1 Nov 2012

the spectral resolution is much better than that measured with the OSA. The optical spectrum in Fig. 3 clearly shows a constant frequency component on the left side for velocity measurement, a residual optical carrier in the middle, and a wideband frequency chirp on the right side for range measurement. In addition, the residual modulation sideband on the opposite side of the optical carrier is also visible, but with >20dB power suppression ratio. Note that there are also a few spectral lines in Fig. 3 which were generated from nonlinear mixing between the residual optical carrier, the single-tone modulation and its unsuppressed sideband. This is attributed to the nonlinear transfer function of the system as well as the saturation of the photodiode since the power of the optical LO in the heterodyne spectral measurement was relatively high.

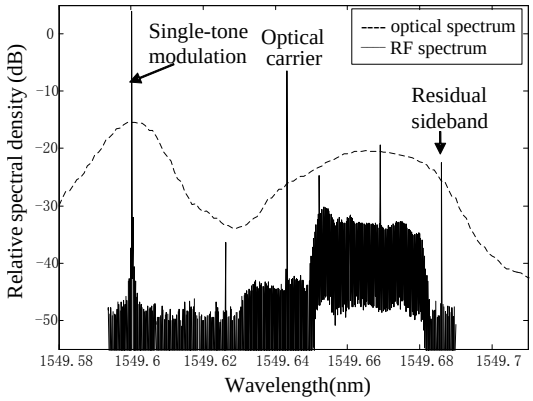

Fig. 3. Signal optical spectrum measured with an OSA with 0.01nm resolution (dashed line) and with coherent heterodyne detection (solid line).

At the lidar receiver, the optical signal reflected from the spinning disc was combined with LO through the 90° optical hybrid. The two output ports are detected by two photodiodes, digitized and combined to reconstruct the complex optical field as described by Eq. (13). With the perspective of real-time lidar operation, we truncated the recorded time-domain digital signal into lengths equal to the pulse repetition time $T' = 1.5298\mu s$, corresponding to the update rate of approximately 653 MHz. This composite signal is converted into frequency domain through an FFT process. Figure 4 shows a typical spectrum of the complex electrical signals measured at the lidar receiver. This figure covering the full spectral window demonstrates the digital recovery of the complex optical field spectrum comparable to that shown in Fig. 3, and the two optical sidebands can be utilized for independent purposes.

Velocity detection is accomplished by measuring the Doppler induced frequency shift of the single-tone on the lower optical sideband. Figure 5 shows the expanded view at that single-tone for the target with a positive and a negative velocity by changing the orientation angle of the spinning disc. In the two measurements, both the radial position of the laser beam on the disc and the distance between the lidar and the disc remain unchanged. The solid line and the dashed line in Fig. 5 represent the spectra of the received signal with the target moving towards and away from the observer, respectively. Because of the Doppler effect, the measured frequency is different from the original single-tone modulation frequency of $f_{CW} = -5.3545GHz$, The precise target velocity information can be obtained by measuring this frequency shift. The bottom and the top horizontal axes of Fig. 5 indicate the frequency f and the corresponding velocity calculated from $v = \left(|f| - |f_{CW}|\right)\lambda/2$. The target velocities indicated by the solid and the dashed spectra are + 5.81m/s and −7.62m/s, corresponding to the disc orientation angle of 32° and −44°, respectively. Based on the 3-dB width of the

#175888 - $15.00 USD Received 10 Sep 2012; revised 20 Oct 2012; accepted 22 Oct 2012; published 1 Nov 2012

spectra, the resolution of the velocity measurement in this experiment is approximately 0.5m/s, which agrees with the theoretical value predicted by $v_{res} = \lambda / (2T')$.

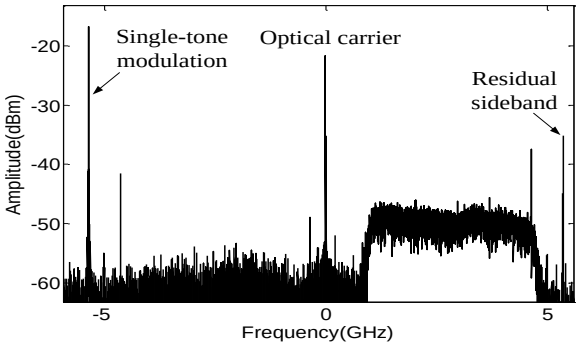

Fig. 4. Power spectral density of the detected complex electrical signal described by Eq. (13).

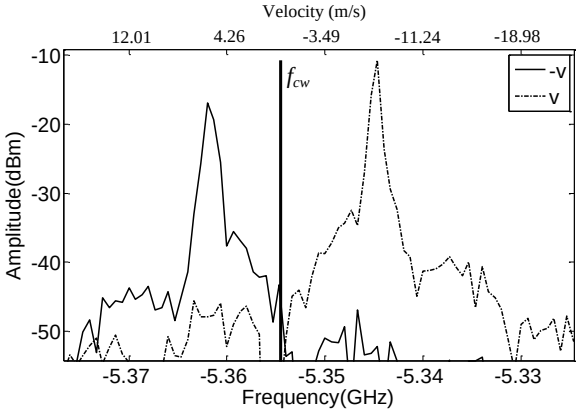

Fig. 5. Zoomed-in view at the single-tone modulation frequency for velocity measurement. Solid and dashed lines represent spectra measured when the target moves toward and away from the observer, respectively.

Figure 6 shows the de-chirped spectra for range measurements. De-chirping was performed by mixing the received signal shown on the upper sideband of Fig. 4 with the original chirping waveform. However, for a moving target, the Doppler-effect shifts the detected signal by a frequency f_d which is a function of the target velocity. Obviously this Doppler frequency shift has an impact on the de-chirping process. The solid and the dashed lines in Fig. 6 represent de-chirped spectra obtained for the target with the positive and the negative speed as discussed previously. The distance between the lidar transmitter and the target can be calculated by,

$$R = (f_R - f_d)cT / 2B \tag{14}$$

Where f_R is the peak frequency of the de-chirped spectrum, f_d is the Doppler frequency shift which is obtained from the velocity measurement described above, and B is the chirping bandwidth. Note that in Fig. 6 there is an extra frequency component at $f_c = 0.43GHz$ in each spectrum but at a much lower amplitude. This is originated from the back reflection off the fiber APC (angled physical contact) terminal which leads to the telescope. Since optical signal reflected from the fiber terminal is not affected by the Doppler frequency shift caused by the target velocity, the peak frequency of this component is identical for the two measurements. In fact, the actual distance between the fiber terminal (at the telescope) and the

#175888 - $15.00 USD Received 10 Sep 2012; revised 20 Oct 2012; accepted 22 Oct 2012; published 1 Nov 2012

target can simply be determined from the frequency difference between the spectral peaks caused by the target and the fiber terminal as $R' = (f_R - f_c - f_d)cT/2B$. This resulted in the target distances (from the fiber terminal) of $R' = 1.614m$ and $R' = 1.612m$ for the measurements with positive and negative velocities of the target, respectively. Apparently the location of the disc was slightly moved in the process of flipping its orientation angle. Based on the 3dB width of the de-chirped spectrum, the range resolution is determined as approximately 2.8cm. This roughly agrees with the calculated range resolution $R_{res} = c/2B = 3.49cm$, where R_{res} is defined as the width between the minima on the two sides of the central peak.

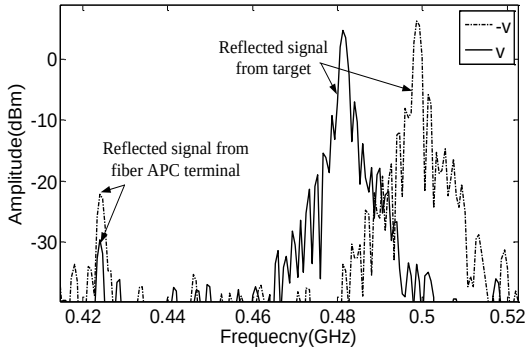

Fig. 6. De-chirped signal spectra for distance measurements. Solid and dashed lines represent spectra measured when the target moves toward and away from the observer, respectively.

4. Conclusion

In this paper, we have demonstrated a coherent lidar system utilizing complex optical field to enhance its functionality and flexibility. An electro-optic I/Q modulator was used in the transmitter to generate the complex optical field modulation, which allowed two independent modulation waveforms to be loaded onto the lower and upper optical sidebands to achieve multiple functionalities. This complex optical field was recovered at the lidar receiver through a 90° optical hybrid. We have experimentally demonstrated the simultaneous detection of target range and vector velocity with high resolution. In comparison to a coherent heterodyne lidar using a conventional AOM as the frequency shifter, electro-optic I/Q modulator intrinsically has a much wider modulation bandwidth, so that it is able to provide unprecedented range resolution and the ability to detect high velocity without spectral aliasing. Because an additional degree of freedom is made available to the optical signal, the proposed technique can be applied to other advanced lidar detection schemes for enhanced functionalities. Note that the requirement of high speed digital electronics in the wideband Lidar proposed here may increase the cost of the system, and therefore a tradeoff between performance and cost has to be made depending on specific applications.

Acknowledgments

This work was supported in part by CIENA Corp, and by KU Transportation Research Institute (TRI). S. Gao acknowledges the financial support from China Scholarship Council (CSC).

#175888 - $15.00 USD Received 10 Sep 2012; revised 20 Oct 2012; accepted 22 Oct 2012; published 1 Nov 2012